Electronic Supplementary Material (ESI) for Journal of Materials Chemistry A.
This journal is © The Royal Society of Chemistry 2024

Supporting Information:

Deciphering the Morphology of Transition Metal Carbonate Cathode Precursors

Pallab Barai[1], Xiaoping Wang[2], Mark Wolfman[3], Jiajun Chen[2], Arturo Gutierrez[2], Juan C. Garcia[2], Jianguo Wen[4], Tiffany Kinnibrugh[2], Timothy T. Fister[2], Hakim H. Iddir[2], and Venkat Srinivasan[5*]

[1]Applied Materials Division, Argonne National Laboratory, Lemont, IL 60439 USA

[2]Chemical Sciences and Engineering Division, Argonne National Laboratory, Lemont, IL 60439 USA

[3]Advanced Photon Source, Argonne National Laboratory, Lemont, IL 60439 USA

[4]Center for Nanoscale Materials, Argonne National Laboratory, Lemont, IL 60439 USA

[5]ACCESS, Argonne National Laboratory, Lemont, IL 60439 USA

Revised version for submission in

Journal of Materials Chemistry A

March 2024

*Corresponding author: Venkat Srinivasan (vsrinivasan@anl.gov)

Computational Methodology

More details of the computational procedure are provided below in the Supplementary Information section.

Equilibrium Calculations: Extent of a particular chemical reaction, and the relation between the concentration of the reactants and the products, are determined from the equilibrium constants. For example, suppose, a chemical reaction between A^+ and B^- leads to a product of AB, and the equilibrium constant for this particular reaction is denoted as K_{AB}, which can also be written as:[1]

$$A^+ + B^- \rightleftharpoons AB, \text{ with equilibrium constant } K_{AB} \qquad \text{(S1)}$$

Then the relation between their concentration and equilibrium constant can be written as:[1, 2]

$$K_{AB} = [AB]/[A^+][B^-] \quad \text{or,} \quad [AB] = K_{AB}[A^+][B^-] \qquad \text{(S2)}$$

Concentration of all the compounds in Eqs. (1) – (5) (in the main manuscript) is written in terms of the equilibrium constants and individual elemental components by following a similar technique demonstrated in Eq. (S2). A list of all the chemical reactions and the magnitude of the corresponding equilibrium constants are provided in Table: S1.

Table: S1. List of equations, and corresponding equilibrium constants, used to determine the composition of the transition metal carbonate precipitates.[3, 4]

List of equations	Equilibrium constants (K_{eq})
$NH_4^+ + OH^- \rightleftharpoons NH_4OH$	6.3095×10^4
$H^+ + CO_3^{2-} \rightleftharpoons HCO_3^-$	1.7793×10^{10}
$H^+ + HCO_3^- \rightleftharpoons H_2CO_3$	2.3255×10^6
$Ni^{2+} + 2OH^- \rightleftharpoons Ni(OH)_2$	1.6595×10^{15}
$Mn^{2+} + 2OH^- \rightleftharpoons Mn(OH)_2$	5.0118×10^{12}
$Co^{2+} + 2OH^- \rightleftharpoons Co(OH)_2$	7.7624×10^{14}
$Ni^{2+} + CO_3^{2-} \rightleftharpoons NiCO_3$	7.0422×10^6
$Mn^{2+} + CO_3^{2-} \rightleftharpoons MnCO_3$	4.2735×10^{10}
$Co^{2+} + CO_3^{2-} \rightleftharpoons CoCO_3$	1×10^{10}
$Ni^{2+} + NH_3 \rightleftharpoons [Ni(NH_3)]^{2+}$	6.4565×10^2
$Ni^{2+} + 2NH_3 \rightleftharpoons [Ni(NH_3)_2]^{2+}$	1.2022×10^5

$Ni^{2+} + 3NH_3 \rightleftharpoons [Ni(NH_3)_3]^{2+}$	7.0794×10^6
$Ni^{2+} + 4NH_3 \rightleftharpoons [Ni(NH_3)_4]^{2+}$	1.3182×10^8
$Ni^{2+} + 5NH_3 \rightleftharpoons [Ni(NH_3)_5]^{2+}$	8.5113×10^8
$Ni^{2+} + 6NH_3 \rightleftharpoons [Ni(NH_3)_6]^{2+}$	1.2022×10^9
$Mn^{2+} + NH_3 \rightleftharpoons [Mn(NH_3)]^{2+}$	10^1
$Mn^{2+} + 2NH_3 \rightleftharpoons [Mn(NH_3)_2]^{2+}$	3.4673×10^1
$Mn^{2+} + 3NH_3 \rightleftharpoons [Mn(NH_3)_3]^{2+}$	5.0118×10^1
$Mn^{2+} + 4NH_3 \rightleftharpoons [Mn(NH_3)_4]^{2+}$	1.9952×10^1
$Co^{2+} + NH_3 \rightleftharpoons [Co(NH_3)]^{2+}$	1.2589×10^2
$Co^{2+} + 2NH_3 \rightleftharpoons [Co(NH_3)_2]^{2+}$	4.6773×10^3
$Co^{2+} + 3NH_3 \rightleftharpoons [Co(NH_3)_3]^{2+}$	6.0255×10^4
$Co^{2+} + 4NH_3 \rightleftharpoons [Co(NH_3)_4]^{2+}$	3.3884×10^5
$Co^{2+} + 5NH_3 \rightleftharpoons [Co(NH_3)_5]^{2+}$	5.6234×10^5
$Co^{2+} + 6NH_3 \rightleftharpoons [Co(NH_3)_6]^{2+}$	1.3803×10^5

Growth Mechanism of Primary Particles and Primary Aggregates: As already pointed out in the main manuscript, formation of the primary aggregates occurs through the nucleation of new primary particles on the surface of the existing primary particles. SEM and TEM images indicate that the transition metal carbonate $(TMCO_3)$ primary aggregates take almost a spherical shape. If the primary aggregate is considered to be a single particle, its growth mechanism can be simulated as the simple precipitation induced growth of a single particle:[5]

$$c_{TMCO_3} \cdot \frac{dr_{ppa}}{dt} = k_{ppa} \cdot \left([TM^{2+}] \cdot [CO^{2-}_3] - K_{SP,TMCO_3} \right) \tag{S3}$$

where, r_{ppa} indicates the radius of the primary particle aggregates, c_{TMCO_3} is the concentration of transition metal carbonate within the precipitated particle, k_{ppa} denotes the reaction rate constant for the precipitation of the $TMCO_3$ for growing the primary particle aggregates, t indicates time, $[TM^{2+}]$ is the concentration of the transition metal cations, $[CO^{2-}_3]$ denotes the concentration of the carbonate anions, and $K_{SP,TMCO_3}$ is the solubility product of the $TMCO_3$ being precipitated. It is possible to rearrange the Eq. (S3), and write it in the following fashion:

$$\frac{dr_{ppa}}{dt} = \frac{k_{ppa} \cdot K_{SP,TMCO_3}}{c_{TMCO_3}} \cdot \left(\frac{[TM^{2+}] \cdot [CO_3^{2-}]}{K_{SP,TMCO_3}} - 1 \right) = \frac{k_{ppa} \cdot c_{eq,TMCO_3}}{c_{TMCO_3}} \cdot \left(SSR_{TMCO_3} - 1 \right) \tag{S4}$$

The modified reaction rate constant k_{ppa} is used in the present context, along with the equilibrium concentration of transition metal carbonates within the solution $\left(c_{eq,TMCO_3}\right)$, can be used to simplify the expression that governs the growth of the primary particle aggregates. As shown in Eq. (S4), the modified expression for the growth of primary particle aggregate is written in terms of the supersaturation ratio of the transition metal carbonate $\left(SSR_{TMCO_3}\right)$, which is defined as:[6]

$$SSR_{TMCO_3} = [TM^{2+}] \cdot [CO_3^{2-}] / K_{SP,TMCO_3} \tag{S5}$$

Note that the equilibrium concentration of transition metal carbonates is extracted from the solubility product according to the following relation:

$$c_{eq,TMCO_3} = \sqrt{K_{SP,TMCO_3}} \tag{S6}$$

In the present research, magnitudes of the solubility product of the transition metal carbonates are assumed to be equivalent to the equilibrium constants corresponding to the same $TMCO_3$ $\left(K_{SP,TMCO_3} = K_{eq,TMCO_3}\right)$, which is reported in Table S1.

Evolution of the primary aggregates occurs through two different processes, growth of individual primary particles, and nucleation of new primary particles on the surface of the existing ones. Surface nucleation occurs because the growth of individual primary particles is slow enough such that the minimization of energy through direct precipitation is not a viable option.[7] Nucleation on top of the surface of the existing primary particles can lead to faster precipitation of the supersaturated transition metal carbonate reactants, and quick growth of the precipitated particles.

Following the expression of growth for the primary particle aggregates (as shown in Eq. (S4)), growth of the individual primary particles through direct precipitation can be captured using the following relations:[5]

$$\frac{dr_{pp}}{dt} = \frac{k_{pp} \cdot c_{eq,TMCO_3}}{c_{TMCO_3}} \cdot \left(SSR_{TMCO_3} - 1\right) \tag{S7}$$

Here, r_{pp} indicates the radius of the primary particles, c_{TMCO_3} is the concentration of $TMCO_3$ within the precipitate, k_{pp} denotes the reaction rate constant for the direct precipitation of $TMCO_3$, and the other terms were already explained earlier while discussing about Eq. (S3) and (S4). The expressions demonstrated in Eq. (S4) for the growth of primary particle aggregates and that demonstrated in Eq. (S7) for the growth of individual primary particles are very similar, with the difference being the reaction rate constants. Since, the growth of the primary particle aggregates occurs much faster than the growth of the primary particles itself, the reaction rate constant for primary particle aggregate (k_{ppa}) is expected to be much larger than the reaction rate constant for the individual primary particles (k_{pp}), which can also be written as $k_{ppa} > k_{pp}$. Altering the transition metal type (Ni^{2+}, Mn^{2+}, or Co^{2+}), as well as the distribution of the various transition metals ($NMC111CO_3$ or Co-free $Ni_xMn_{1-x}CO_3$), can lead to substantially different magnitudes of the reaction rate constants for the growth of primary particle aggregates and individual primary particles.[8] In other words, k_{ppa} and k_{pp} are functions of the type of transition metal (TM^{2+}) present within the solution.

For capturing the surface nucleation density (J_{sn}) of the $TMCO_3$ primary particles, rate of surface nucleation density is given as:[6, 9]

$$\frac{dJ_{sn}}{dt} = k_{sn} \cdot SSR_{TMCO_3} \tag{S8}$$

where, k_{sn} indicates the rate coefficient for surface nucleation density with the unit of $\#/m^2s$, and the rest of the terms have already been described earlier. Changing the transition metal type can substantially alter the magnitude of the supersaturation ratio $\left(SSR_{TMCO_3}\right)$, as well as the reaction rate constant for the surface nucleation process (k_{sn}). Note that the surface nucleation density (J_{sn}) demonstrates the unit of $\#/m^2$. These rate coefficients for surface nucleation (k_{sn}) and the supersaturation ratio $\left(SSR_{TMCO_3}\right)$ are used in Eq. (11) and (12), in the main manuscript, for determining the domain searched by the transition metal ions for a minimum energy location, before precipitating as a surface nucleus. Also, note that the formation of the morphology of the primary particle aggregates depends more on the reaction rate constant for the primary particle growth (k_{pp}) and the reaction rate constant for the surface nucleation processes (k_{sn}), and is independent of the reaction rate constant used for the growth of the primary particle aggregates (k_{ppa}). Magnitudes of the various reaction rate constants, such as, k_{ppa}, k_{pp}, and k_{sn}, and the transition metal diffusion coefficients (D_{TM}), for the precipitation of different transition metal carbonates, used in the present simulation are provided in Table: S2.

Table: S2. Reaction rate constants used for capturing the growth of the primary particles through direct precipitation (k_{pp}), growth of primary particle aggregates (k_{ppa}), and rate constant for the surface nucleation processes (k_{sn}):[10-13]

Various Parameters	Units	Ni^{2+}	Co^{2+}	$NMC111$
Reaction rate constant for direct precipitation on primary particles (k_{pp})	m/s	1×10^{-7}	2×10^{-7}	4×10^{-7}
Reaction rate constant for the surface nucleation process (k_{sn})	$\#/m^2s$	4×10^{6}	1.25×10^{3}	2×10^{2}
Reaction rate constant for the growth of primary particle aggregates (k_{ppa})	m/s	2×10^{-5}	1×10^{-6}	1×10^{-6}
Diffusion coefficient of the transition metals in the reacting solution (D_{TM})	m^2/s	7×10^{-10}		

Simulating Evolution of the Secondary Particles: Four different physical phenomena are modeled to simulate the formation and growth of the secondary particles:[10, 14]

i) Nucleation of the primary particle aggregates.

ii) Growth of the primary particle aggregates.

iii) Random movement of the primary particle aggregates through stirring induced convection and/or diffusion processes.

iv) Agglomeration of the primary particle aggregates with other primary aggregates or other secondary particles, which leads to the formation and growth of the secondary particles, respectively.

Mathematical expressions used to model these four physical phenomena will be discussed next.

Nucleation of primary particles: The standard classical nucleation theory (CNT), developed to capture the homogeneous nucleation of particles, is adopted in the present study to simulate the formation of primary particles, and their aggregates, within the reacting solution. According to this theory, the rate of nucleation of primary particles (J_{pp}) is given by:[9, 15]

$$J_{pp} = J_{pp,0} \cdot \exp\left(16\pi\gamma_{sl}^3\bar{V}^2/\left(3k_B R^2 T^3 \cdot (\ln SSR)^3\right)\right) \qquad \text{(S9)}$$

where, $J_{pp,0}$ indicates the total number of available nucleation sites, γ_{sl} is the surface energy between the solid precipitate and the reactor liquid, $\bar{V}$ is the partial molar volume of the precipitating species, k_B indicates the Boltzmann's constant, R is the universal gas constant, and T denotes temperature. The total number of available nuclei $(J_{pp,0})$ is obtained from the relation,[6, 10]

$$J_{pp,0} = \frac{1}{\bar{V}} \cdot \sqrt{\frac{N_a RT}{\gamma_{sl}}} \cdot D_{TM} c_{eq} \cdot SSR \cdot \ln SSR \qquad \text{(S10)}$$

where, N_a indicates the Avogadro constant, D_{TM} is the diffusivity of the transition metal ions within the reacting liquid, c_{eq} is the equilibrium concentration of the transition metal carbonate within the reacting solution before the precipitation initiates (which is already defined in Eq. (S6)), and SSR is the supersaturation ratio of the $TMCO_3$ within the reactor (already defined in Eq. (S5)). The rate of nucleation (J_{pp}) is given in the units of $\#/(m^3 \cdot s)$, which is also the unit of the total number of available nuclei $(J_{pp,0})$. Increase in the total number of primary particle nuclei over a time interval (Δt) is estimated as:[10]

$$J_{pp}(t + \Delta t) = J_{pp}(t) + \dot{J}_{pp} \cdot \Delta t \tag{S11}$$

where, $J_{pp}(t)$ and $J_{pp}(t + \Delta t)$ is the number density of the primary particle nuclei (with units of $\#/m^3$) at time t and $t + \Delta t$. All the parameters used to estimate the nucleation density of primary particles are provided in Table S3.

Growth of the primary particle aggregates: After the nucleation of the primary particle, their growth leads to the formation and evolution of the primary particle aggregates. It is very important to appropriately predict the growth of these primary particle aggregates because both the rate of diffusion and the rate of agglomeration depend strongly on their size.[2] In the present context, due to the very high diffusivity of the reactants within the solution, rate limited growth of the primary particle aggregates is assumed.[12] The set of equations provided in Eqs. (S3) – (S6) is solved to capture the increase in size of the primary particle aggregates. The parameters used to solve these equations are provided in Table S3. Due to the very high diffusivity of the transition metal and carbonate ions within the reacting solution, the bulk concentration of these ions is used in the growth simulations. This simplification helps to eliminate the calculations associated with solving for the diffusion induced concentration gradients of the reacting ions within the solution, which effectively makes the simulations much faster.

Random movement of the primary particle aggregates: Movement of the primary particle aggregates, as well as the secondary particles, is simulated using a Kinetic Monte Carlo (KMC) approach. At each time step, a particle is allowed to move to its nearest, or second nearest, neighbors, through either convective motion, or Stokes-Einstein diffusion process. The liquid velocity (v_{liq}) for convection is assumed to be an input parameter, which affects particle of all sizes equivalently. The Stokes-Einstein diffusivity (D_{SE}) is written as:[2]

$$D_{SE} = (k_B T)/(6\pi\eta r_{particle}) \tag{S12}$$

where, η indicates the viscosity of the reacting solution, and $r_{particle}$ is the radius of the particles, which can be either a primary particle aggregate, or a secondary particle. The time (t_{move}) taken by each particle to move to its nearest (or second nearest) neighbor is given as:

$$t_{move} = \min\left((d^2/D_{SE}),(d/v_{liq})\right) \tag{S13}$$

where, d is the distance to the nearest, or second nearest, neighbor. It is assumed that the faster of the two processes, diffusion or convection, dominates the transport of the particles. The rate associated with each move $(rate_{move})$ is estimated as the reciprocal of the time (t_{move}) required for that particular move:

$$rate_{move} = 1/t_{move} \tag{S14}$$

Finally, the Kinetic Monte Carlo scheme is implemented by adding all the rates, and randomly selecting one of them, while the time increment is estimated using a random number and the summation of all the rates associated with all the processes.[16] Again, the parameters used for running the simulations are provided in Table S3.

Agglomeration and growth of secondary particles: During their random movement if a primary particle aggregate, or a secondary particle, encounters another primary particle aggregate, or another secondary particle, there is a possibility that due to the collision between them, they

will stick to each other because agglomeration leads to minimization in the overall system energy.[17] Energy associated with each particle $(E_{particle})$ is estimated as:

$$E_{particle} = V\gamma_{sl}/r_{particle} \tag{S15}$$

Here, V indicates molar volume of the particle, γ_{sl} is the interfacial energy between the solid and the liquid, and $r_{particle}$ denotes the particle radius. The probability of agglomeration $(prob_{agg})$ experienced by each particle is defined as:

$$prob_{agg} = \exp\left(-E_{particle}/RT\right) \tag{S16}$$

where, R is the universal gas constant, and T is the temperature in the Kelvin scale. The energy associated with each secondary particle or primary particle aggregate $(E_{particle})$ is estimated from Eq. (S15). During the collision of two different particles, probability of agglomeration experienced by the one with smaller size is considered. Smaller particles contain larger surface energy $(E_{particle,small} > E_{particle,large})$ and the magnitude of their probability of agglomeration $(prob_{agg,small} < prob_{agg,large})$ is also smaller. If this particular probability of agglomeration experienced by the smaller particle is less than a randomly selected number, the two particles are assumed to agglomerate, and move together according to their random movement mechanism. Otherwise, the two particles remain as separate entities. Note that no upper limit to the size of the secondary particles is assigned in the present simulation. Also, note that fluid shear induced breakage of particles is not considered here.[17, 18]

Table: S3. List of parameters used for simulating the evolution of the secondary $NMC111CO_3$ precursor particles, through the nucleation, growth, and agglomeration mechanisms, is provided below.

Parameter	Symbol	Unit	Value	Reference
Solubility product	$K_{SP,TMCO_3}$	$(mol/m^3)^2$	6.9262×10^{-10}	[4]
Reaction rate for the growth of primary particle aggregates	k_{ref} or k_{ppa}	m/s	1×10^{-6}	Fitted
Concentration inside particle	c_{TMCO_3}	mol/m^3	32200.0	[19]
Temperature	T	K	323.15	Experiments
Stirring induced convective velocity	v_{liq}	m/s	10^{-5}	Fitted
Surface energy density	γ_{sl}	J/m^2	1.46	DFT calculations
Boltzmann constant	k_B	J/K	1.3806×10^{-23}	--
Viscosity of reacting solution	η	$Pa \cdot s$	8.9×10^{-4}	[20]
Partial molar volume of precipitated $TMCO_3$	$\bar{V}$	m^3/mol	31.0667×10^{-6}	[19]

Table S4. Surface Energies for Selected Surfaces for NMC111 Under a Stoichiometric Ratio of the Species

	Surface Orientation	**$MnCO_3$**	**$NiCO_3$**	**$CoCO_3$**
Surface energy (J/m^2)	(102)	1.05	1.53	1.79
	(104)	1.77	1.92	1.98
	(001)	1.55	1.94	2.05
	(100)	2.21	2.43	2.51

Additional Figures

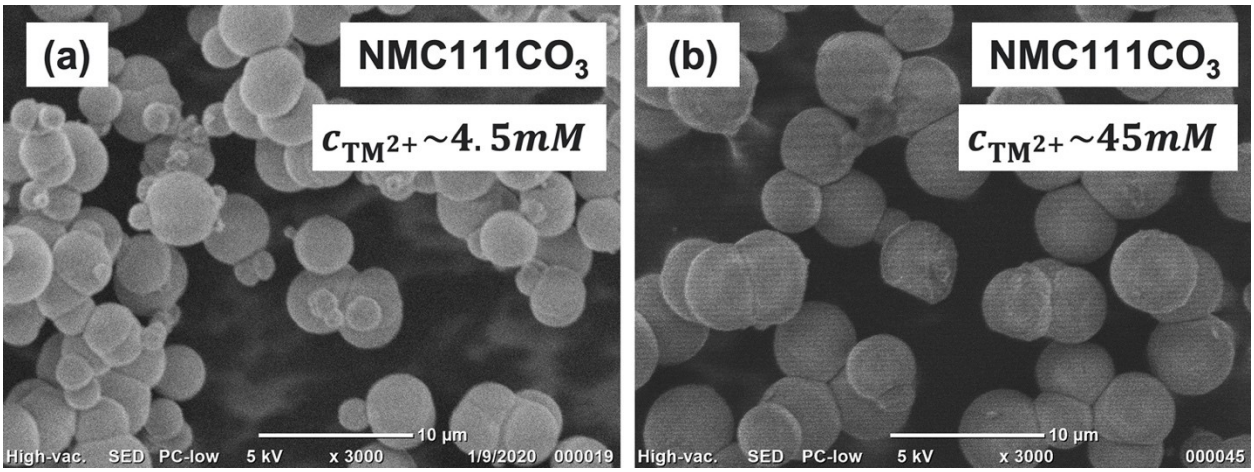

Figure: S1. SEM images of $NMC111CO_3$ precursors with ammonia over transition metal ratio ($[NH_4]$:[TM]) of 40:1. (a) Transition metal concentration kept constant at 4.5 mM. (b) Transition metal concentration kept constant at 45 mM. The scale bar is constant in both images, which is equivalent to 10 µm. It is evident that increasing transition metal concentration from 4.5 mM to 45 mM leads to an increase in the secondary particle sizes. It appears that the average particle sizes increase from 4.25 µm to 5.5 µm as the metal concentration increases from 4.5 mM to 45 mM in the reacting solution.

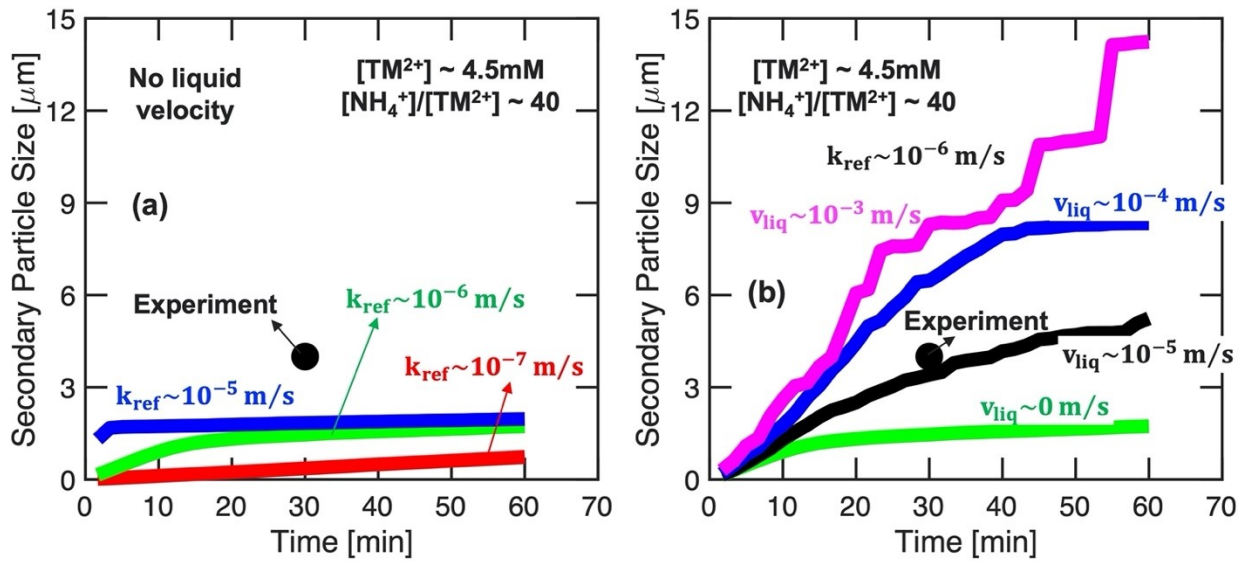

Figure: S2. Influence of the reaction rate constant (k_{ref}) and the liquid velocity (v_{liq}) in determining the secondary particle size as predicted by the Kinetic Monte Carlo (KMC) based computational scheme. Coprecipitation assumed to occur in a batch mode with transition metal concentration around 4.5 mM and ammonia over metal ([NH_4]:[TM]) ratio of 40:1. The experimentally observed secondary particle size is denoted by the black circle. (a) Impact of the reaction rate constant (k_{ref}) without any liquid velocity $(v_{liq}\sim 0)$ shows that increasing the reaction rate constant cannot increase the secondary particles size substantially without the help of liquid velocity. (b) Evolution in secondary particle size with time while keeping the reaction rate constant fixed at 10^{-6} m/s $(k_{ref}\sim 10^{-6} m/s)$. It is evident that extremely large velocities can lead to very big secondary particles, whereas liquid velocity around 10^{-5} m/s $(v_{liq}\sim 10^{-5} m/s)$ leads to a good correlation with the experimental observations. All the subsequent analysis of secondary particle growth will use $k_{ref}\sim 10^{-6} m/s$ and $v_{liq}\sim 10^{-5} m/s$ as they provide the best correlation with the experimental observations.

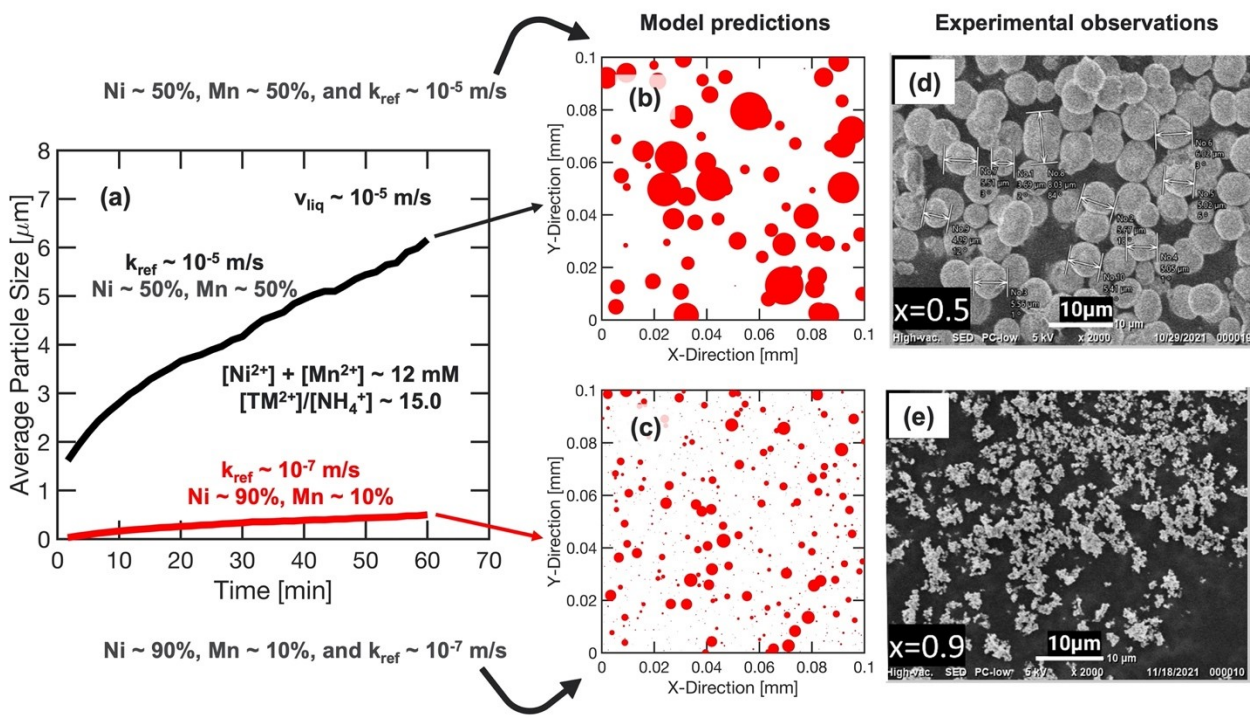

Figure: S3. Application of the developed Kinetic Monte Carlo (KMC) methodology for predicting the secondary particle sizes observed in other transition metal carbonates. (a) Comparing the model predicted average secondary particle size for equal amount of Ni and Mn (black line) with 90% Ni containing precipitates (red line). The total TM content is kept fixed at 12 mM, and ammonia over TM ratio is 15. Higher magnitude of reaction rate constant (k_{ref}) is assumed for the Mn-rich precipitates. (b) and (c) Computationally predicted size distribution of secondary particles for 50% Mn and 10% Mn, respectively. (d) and (e) Corresponding experimental observations for precipitates with 50% Mn and 10% Mn, where the precipitates with larger Mn content leads to significantly larger secondary particle sizes. The experimental results are obtained by precipitating the $TMCO_3$ according to the abovementioned conditions in a batch reactor for 1 hour. Note that no cobalt (Co) is used in any of these two precipitates.

References

1. Dean, J.A. and N.A. Lange, *Lange's handbook of chemistry*. 1973, McGraw-Hill: New York. p. volumes.
2. Deen, W.M., *Analysis of transport phenomena*. Topics in chemical engineering. 1998, New York: Oxford University Press. xix, 597 p.
3. van Bommel, A. and J.R. Dahn, *Analysis of the Growth Mechanism of Coprecipitated Spherical and Dense Nickel, Manganese, and Cobalt-Containing Hydroxides in the Presence of Aqueous Ammonia.* Chemistry of Materials, 2009. **21**(8): p. 1500-1503.
4. Wang, D., et al., *Growth mechanism of Ni0. 3Mn0. 7CO3 precursor for high capacity Li-ion battery cathodes.* Journal of Materials Chemistry, 2011. **21**(25): p. 9290-9295.
5. Thanh, N.T., N. Maclean, and S. Mahiddine, *Mechanisms of nucleation and growth of nanoparticles in solution.* Chemical reviews, 2014. **114**(15): p. 7610-7630.
6. Kashchiev, D. and G. Van Rosmalen, *Nucleation in solutions revisited.* Crystal Research and Technology: Journal of Experimental and Industrial Crystallography, 2003. **38**(7-8): p. 555-574.
7. Navrotsky, A., *Nanoscale effects on thermodynamics and phase equilibria in oxide systems.* ChemPhysChem, 2011. **12**(12): p. 2207-2215.
8. Dong, H. and G.M. Koenig Jr, *Compositional control of precipitate precursors for lithium-ion battery active materials: role of solution equilibrium and precipitation rate.* Journal of Materials Chemistry A, 2017. **5**(26): p. 13785-13798.
9. Karthika, S., T.K. Radhakrishnan, and P. Kalaichelvi, *A Review of Classical and Nonclassical Nucleation Theories.* Crystal Growth & Design, 2016. **16**(11): p. 6663-6681.
10. Barai, P., et al., *Multiscale computational model for particle size evolution during coprecipitation of Li-ion battery cathode precursors.* The Journal of Physical Chemistry B, 2019. **123**(15): p. 3291-3303.
11. Garcia, J.C., et al., *Predicting morphological evolution during coprecipitation of MnCO3 battery cathode precursors using multiscale simulations aided by targeted synthesis.* Chemistry of Materials, 2020. **32**(21): p. 9126-9139.
12. Sato, H., M. Yui, and H. Yoshikawa, *Ionic diffusion coefficients of Cs+, Pb2+, Sm3+, Ni2+, SeO2-4 and TcO− 4 in free water determined from conductivity measurements.* Journal of Nuclear Science and Technology, 1996. **33**(12): p. 950-955.
13. Zeebe, R.E., *On the molecular diffusion coefficients of dissolved CO2, HCO3-, and CO32- and their dependence on isotopic mass.* Geochimica et Cosmochimica Acta, 2011. **75**(9): p. 2483-2498.
14. Ring, T.A. *Nucleation. Growth and Agglomeration during Precipitation of Powders*. in *Proceedings of Second World Congress PARTICLE TECHNOLOGY*. 1990. Kyoto, Japan.

15. Vetter, T., et al., *Modeling nucleation, growth, and Ostwald ripening in crystallization processes: a comparison between population balance and kinetic rate equation.* Crystal growth & design, 2013. **13**(11): p. 4890-4905.
16. Burghaus, U., *A practical guide to Kinetic Monte Carlo simulations and classical molecular dynamics simulations : an example booklet*. 2006, New York: Nova Science Publishers. xi, 194 p.
17. Serra, T., J. Colomer, and X. Casamitjana, *Aggregation and breakup of particles in a shear flow.* Journal of Colloid and Interface Science, 1997. **187**(2): p. 466-473.
18. Harshe, Y.M. and M. Lattuada, *Breakage Rate of Colloidal Aggregates in Shear Flow through Stokesian Dynamics.* Langmuir, 2012. **28**(1): p. 283-292.
19. Jain, A., et al., *Commentary: The Materials Project: A materials genome approach to accelerating materials innovation.* APL materials, 2013. **1**(1).
20. Kestin, J., M. Sokolov, and W.A. Wakeham, *Viscosity of liquid water in the range− 8 C to 150 C.* Journal of physical and chemical reference data, 1978. **7**(3): p. 941-948.